

REPORT DOCUMENTATION PAGE

Form Approved
OMB No. 0704-0188

Public reporting burden for this collection of information is estimated to average 1 hour per response, including the time for reviewing instructions, searching existing data sources, gathering and maintaining the data needed, and completing and reviewing this collection of information. Send comments regarding this burden estimate or any other aspect of this collection of information, including suggestions for reducing this burden to Department of Defense, Washington Headquarters Services, Directorate for Information Operations and Reports (0704-0188), 1215 Jefferson Davis Highway, Suite 1204, Arlington, VA 22202-4302. Respondents should be aware that notwithstanding any other provision of law, no person shall be subject to any penalty for failing to comply with a collection of information if it does not display a currently valid OMB control number. **PLEASE DO NOT RETURN YOUR FORM TO THE ABOVE ADDRESS.**

1. REPORT DATE (DD-MM-YYYY) 21-05-2007		2. REPORT TYPE Technical Paper		3. DATES COVERED (From - To)	
4. TITLE AND SUBTITLE Differential Sputter Yields of Boron Nitride, Quartz, and Kapton Due to Low Energy Xe⁺ Bombardment (Preprint)				5a. CONTRACT NUMBER	
				5b. GRANT NUMBER	
				5c. PROGRAM ELEMENT NUMBER	
6. AUTHOR(S) A.P. Yalin, B. Rubin, S.R. Domingue, Z. Glueckert, J.D. Williams (Colorado State Univ.)				5d. PROJECT NUMBER 48470052	
				5e. TASK NUMBER	
				5f. WORK UNIT NUMBER	
7. PERFORMING ORGANIZATION NAME(S) AND ADDRESS(ES) Air Force Research Laboratory (AFMC) AFRL/PRSS 1 Ara Road Edwards AFB CA 93524-7013				8. PERFORMING ORGANIZATION REPORT NUMBER AFRL-PR-ED-TP-2007-274	
9. SPONSORING / MONITORING AGENCY NAME(S) AND ADDRESS(ES) Air Force Research Laboratory (AFMC) AFRL/PRS 5 Pollux Drive Edwards AFB CA 93524-7048				10. SPONSOR/MONITOR'S ACRONYM(S)	
				11. SPONSOR/MONITOR'S NUMBER(S) AFRL-PR-ED-TP-2007-274	
12. DISTRIBUTION / AVAILABILITY STATEMENT Approved for public release; distribution unlimited (PA #07230A)					
13. SUPPLEMENTARY NOTES For presentation at the 43 rd AIAA/ASME/SAE/ASEE Joint Propulsion Conference, Cincinnati, OH, 8-11 July 2007.					
14. ABSTRACT In this contribution we present results of differential sputter yield measurements of boron nitride, quartz, and kapton due to bombardment by xenon ions. The measurements are made using a sputtering diagnostic based on a quartz crystal microbalance (QCM). The QCM measurement allows full angular resolution, i.e. differential sputtering yield measurements are measured as a function of both polar angle and azimuthal angle. Measured profiles are presented for 100, 250, 350 and 500 eV Xe ⁺ bombardment at 0°, 15°, 30° and 45° angles of incidence. We fit the measured profiles with Modified Zhang expressions using two free parameters: the total sputter yield, Y, and characteristic energy E*. Total yields are calculated from the differential profiles and are compared with published values and weight loss values where possible.					
15. SUBJECT TERMS					
16. SECURITY CLASSIFICATION OF:			17. LIMITATION OF ABSTRACT	18. NUMBER OF PAGES	19a. NAME OF RESPONSIBLE PERSON
a. REPORT	b. ABSTRACT	c. THIS PAGE			Dr. Justin W. Koo
Unclassified	Unclassified	Unclassified	SAR	16	19b. TELEPHONE NUMBER (include area code) N/A

Differential Sputter Yields Of Boron Nitride, Quartz, and Kapton Due to Low Energy Xe⁺ Bombardment (Preprint)

A.P. Yalin^{*}, B. Rubin[†], S.R. Domingue[‡], Z. Glueckert[§], J.D. Williams^{**}
Colorado State University, Fort Collins, CO, 80523

In this contribution we present results of differential sputter yield measurements of boron nitride, quartz, and kapton due to bombardment by xenon ions. The measurements are made using a sputtering diagnostic based on a quartz crystal microbalance (QCM). The QCM measurement allows full angular resolution, i.e. differential sputtering yield measurements are measured as a function of both polar angle and azimuthal angle. Measured profiles are presented for 100, 250, 350 and 500 eV Xe⁺ bombardment at 0°, 15°, 30° and 45° angles of incidence. We fit the measured profiles with Modified Zhang expressions using two free parameters: the total sputter yield, Y , and characteristic energy E^* . Total yields are calculated from the differential profiles and are compared with published values and weight loss values where possible.

Nomenclature

y	= differential sputtering yield
E^*	= characteristic energy to describe sputtering profile
M_i	= molar mass of species i
Y	= total sputter yield
Y_{Cond}	= total volumetric sputter yield due to condensable components (lower bound on target yield)
Y_{Target_Max}	= total volumetric sputter yield assuming all sputtering as atoms (upper bound on target yield)
α	= QCM sensor polar angle from target normal
β	= ion incidence angle from target normal
ϕ	= azimuthal angle in the target plane from the plane containing the ion beam and target normal
ρ	= density of target material

I. Introduction

Ion sputtering is the process in which atoms (and molecules, clusters, or ions) are ejected from the surface of a material due to bombarding incident ions¹. Details of the sputtering process are of interest from both theoretical and applied points of view. In this contribution, our interest is in the role of sputtering in electric propulsion (EP) thrusters used for satellite and space exploration²⁻⁸. In these devices, sputter erosion places a fundamental limitation on lifetimes. For example, in ion thrusters the erosion of accelerator grids is critical, while in Hall thrusters it is the erosion of insulator channels that can play a key role. Materials of interest include refractory metals as well as multicomponent materials such as boron nitride, quartz, and kapton. Additionally, sputtered particles from within the thrusters or from external spacecraft components can redeposit and contaminate spacecraft surfaces (e.g. thermal control surfaces).

Owing to relatively long lifetimes (5-10+ years) of EP thruster devices and the complexity and expense of experimental tests, effects of sputter erosion and redeposition are generally studied with numeric codes. For erosion studies (lifetime), one aims to compute the amount of surface erosion due to the bombarding ions. The calculation requires knowledge of the total sputter yields (Y) of the eroding materials of interest. Modeling of redeposition

^{*} Assistant Professor, Mechanical Engineering, Colorado State University, AIAA Member.

[†] Post-Doctoral Research Associate, Mechanical Engineering, Colorado State University.

[‡] Undergraduate Research Associate, Mechanical Engineering, Colorado State University.

[§] Undergraduate Research Associate, Mechanical Engineering, Colorado State University.

^{**} Assistant Professor, Mechanical Engineering, Colorado State University, AIAA Member.

(contamination) additionally requires knowledge of the differential (angular) sputter yields ($y(\alpha, \phi)$) of the eroded materials in order to track the trajectories of the sputtered particles. Total and differential sputter yield profiles have been measured with a multitude of techniques, a partial list of which includes: weight loss⁹, collector plates¹⁰⁻¹¹, mass spectrometry¹², quartz crystal microbalance^{3-7,13-14}, Rutherford backscattering¹⁵⁻¹⁶, radioactive tracers¹⁷, and cavity ring-down spectroscopy¹⁸. The current measurement system builds upon our previous work using a quartz crystal microbalance (QCM) for sensitive measurements of angularly resolved differential sputter yields⁵⁻⁷. By moving the QCM to different angular positions we obtain the differential sputter yield over the full (2π) hemisphere above the target.

Ion sputtering in EP applications is generally by low energy ions (keV and below). At these conditions, stopping is predominantly due to elastic (nuclear) collisions and the sputtering is generally in the linear cascade regime (emitted particles are secondary or higher generation recoils) or single knock-on regime (emitted particles are primary recoils)¹. A classical theory for the linear cascade regime was originally developed by Sigmund¹⁹. Independent of ion incidence angle, the original theory predicts sputtering profiles that are azimuthally symmetric and approximately diffuse in shape, corresponding to cosine-like profiles of the form $y \propto \cos(\alpha)^n$ ($n=1$ for a diffuse profile). More recent theories, as well as experimental and numerical studies show a range of profile shapes. For normally incident ions on polycrystalline and amorphous targets, cosine-like profiles are generally observed with increasingly under-cosine shapes as ion energy is lowered and increasingly over-cosine shapes for higher ion energies^{5-7,12,20-22}. In comparison to a diffuse profile, an under-cosine profile ($n < 1$) has less sputtering in the surface normal direction and correspondingly more sputtering (with the maximum) at intermediate angles. Conversely, an over-cosine profile ($n > 1$) has increased sputtering (and the maximum) in the surface normal direction. For obliquely incident ions at relatively high ion energy, observed profiles also tend to be azimuthally symmetric. However, for lower ion energies the measured profiles tend to be asymmetric with increased sputtering in the forward direction^{5-7,13,17,20}. Similar profiles have been modeled on a theoretical basis²³⁻²⁵.

Our recent research efforts have led to the development of an experimental apparatus and methodologies to measure differential sputter yield profiles due to low energy bombarding ions⁵⁻⁷. The measurement approach is based on a QCM apparatus that moves above the target to measure angularly resolved differential sputter yields. In Section II we briefly summarize the QCM apparatus including recent improvements to the system. We also describe the use of Modified Zhang (MZ) expressions as a means to describe the measured profiles. In Sections III, IV, and V we present sputtering results for bombardment of xenon ions on boron nitride, quartz, and kapton respectively. The profiles are measured at a range of ion energies (100, 250, 350, and 500 eV) and incidence angles (0, 15, 30, and 45 degrees) and clearly show both non-cosine as well as anisotropic sputtering profiles. Where possible, total sputter yields found from integration of the differential sputter yield profiles are compared with published values as well as weight loss values obtained in our laboratory. Finally, conclusions are given in Section VI.

II. Experimental

A. Overview of QCM Measurement System

The experimental apparatus is shown in Figure 1. The system has been previously described⁵⁻⁷ so that in this subsection we give an overview of its essential features, while the following subsection details recent modifications. The ion source and QCM are housed within a 0.125 m³ stainless steel vacuum chamber (43 cm ID x 76 cm long main section), equipped with a 1500 liter/s CTI-8 cryogenic pump. The chamber base pressure was 5×10^{-7} Torr (after an 8-hour bake out prior to measurements) giving a working pressure of approximately 0.6 to 1×10^{-4} Torr. The ion source is based on a discharge chamber operated with xenon gas at typical flowrates of 0.3 to 0.5 sccm. A tungsten hot-filament cathode ionizes the neutral gas and a two-grid ion optic system extracts and focuses the ion beam onto the target. Neutralization of the beam and surface charging effects are addressed in Section II.B. The discharge voltage (V_D) was set between 30 V and 38 V to minimize the number of multiply charged ions produced. Full-width-at-half-maximums (FWHMs) of the ion beams were in the vicinity of 3 cm (at target plane) with peak current densities of approximately 0.3 mA/cm² and average current densities (over the area containing 90% of the beam current) of approximately 0.1 mA/cm² (see Reference 5).

A rotatable target-mount is positioned 23 cm downstream of the ion source. Details of the targets used (HBC grade BN, quartz, and kapton) are presented in Sections III-V. All targets are poly-crystalline (random grain orientations) so that crystallographic orientation effects are not observed. The targets were cleaned using an acetone solution but not mechanically polished. Prior to measurements, new targets were sputter-cleaned for 3-6 hours with

a 500 eV ($\sim 0.2 \text{ mA/cm}^2$) beam from the ion source. The same targets were often used in multiple tests; thus, we have deliberately studied pre-sputtered as opposed to new (un-sputtered) targets to better represent the conditions found in long-duration EP operating applications or in ground-based sputter coating tools. An order-of-magnitude estimate for the typical dose of incident ions (on the target prior to a given test) is approximately 10^{20-21} ions/cm² (corresponding to 10s-100s of hours and eroded thickness of approximately 10-100 microns). Target contamination effects are estimated to be negligible, since for typical conditions the flux of ions incident on the target is approximately 10 times higher than the flux of nitrogen (the major contaminant) to the target⁷.

In deposition mode, the QCM allows determination of differential sputter yields through measurement of mass accumulation (of sputtered particles) on its surface. Mass changes are inferred from changes in the resonant frequency of the crystal. Knowing the change of mass, incident dose of ions, and geometry, the differential sputter yield can be simply calculated. For condensable components, sticking coefficients are assumed to be unity. We also account for noncondensable components as discussed in Sections 3-5. Temperature control on the QCM is discussed in Section II.B.

The angles used to describe the direction of ion incidence and the ejections angles of sputtered particles are shown in figure 1. We define as follows: β is the incidence angle of bombarding ions measured relative to the surface normal ($\beta=0$ for normal incidence), α is the ejection polar angle of sputtered atoms measured relative to the surface normal, and ϕ is the ejection azimuthal angle of the sputtered atoms measured in the plane of the target surface (defined so that $\phi=0$ is in the forward sputter direction i.e. in the direction of the plane containing the surface normal and the incident ion directions). For a given incidence angle (obtained by tilting the target), the differential sputtering profile is obtained by measuring the sputter yield at a series of angles above the target (~ 36 positions).

At a given measurement point, the volumetric differential sputter yield, $y(\alpha, \phi)$, is determined using equation (1), in which $R(\alpha, \phi)$ is the measured mass accumulation rate (found from a deposition monitor device), ρ is the density of target material, $J_{B,avg}$ (C/s) is the ion current incident on the target (measured every 0.5 s and averaged), r_{qcm} the distance from the target center to the QCM (17.4 cm), and A_s is the QCM sensor area (0.535 cm²). The quantity A_s/r_{qcm}^2 corresponds to the solid angle that the QCM sensor subtends while $R(\alpha, \phi)/\rho J_{B,avg}$ corresponds to the volume of sputtered material per bombarding charge. The resulting $y(\alpha, \phi)$ is in units of volume/charge/steradian (e.g. mm³/C/sr). Note that because we study multicomponent materials (where the identity of the sputtering and depositing particles is not always clear), we use volumetric units of differential sputter yield as opposed to atomic based yields. This treatment is further addressed in Sections III-V.

$$y(\alpha, \phi) = \left[R(\alpha, \phi) r_{qcm}^2 \right] / \left[\rho J_{B,avg} A_s \right] \quad (1)$$

In principle, owing to the finite size of the QCM crystal and beam spot on the target, each of our measurements (i.e. QCM positions) corresponds to a (small) range of polar and azimuthal angles joining the target and QCM. We have performed a simple simulation to show that for our geometry and sputter conditions these effects are negligible (worst case of 5% error), so that we can treat our target and QCM as points (not areas) joined by a single vector⁵. We also note that the viewing angle of the QCM is approximately 5.4 steradian (cone apex angle of 165°) which corresponds to an area on the target that is larger than the irradiated area (also a necessary requirement for equation (1)).

B. Modification of QCM Apparatus

We have worked with colleagues at Sigma Instruments to improve our QCM system. For improved measurement sensitivity we have obtained a Sigma Instrument SQC-339 Deposition Controller that reads the crystal

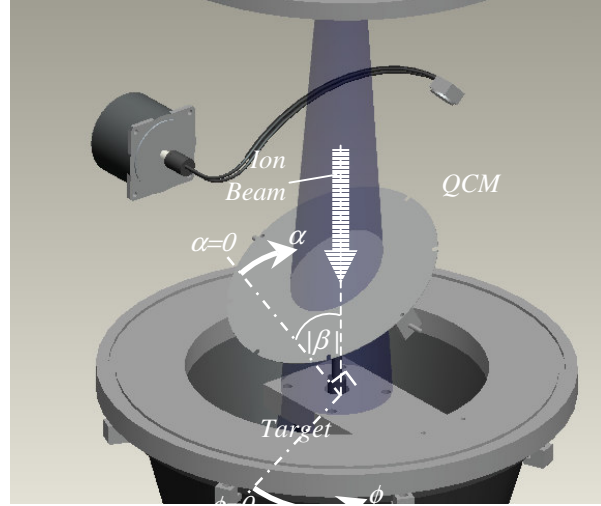


Figure 1. Schematic diagram of experimental setup.

frequency to 0.01 Hz. Also, for improved sensitivity and accuracy a new advanced RC-cut QCM was obtained instead of the conventional AC-cut QCM. The RC-cut QCM manufactured by Tangidyne Corporation is extremely accurate for deposition of very thin films. High sensitivity is achieved by adjusting the stress coefficients of the quartz plate using advanced fabrication methods. The comparison of the QCM mass change during a measurement at fixed sputtering conditions using the old and new QCM is presented at Figure 2. The vertical axis is deposited mass, which should increase linearly against charge (ions sputtering the target). The data set measured using the AC-cut QCM has a relatively high noise level, which is characteristic of this QCM type and significantly reduces measurement sensitivity, especially at low ion energies. For most materials of interest, the new RC-cut QCM enables measurement of differential sputter yield at ion energies as low as 50-100 eV.

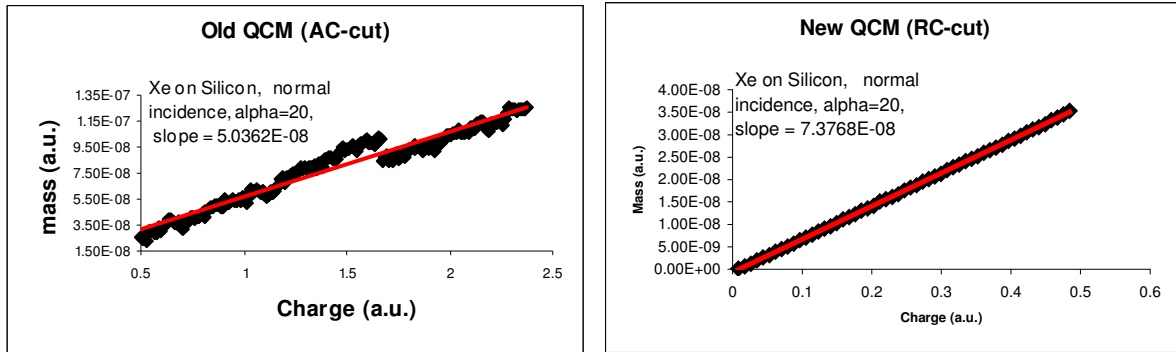


Figure 2 Left/Right: Mass change with old/new QCM. Xe ions on quartz at 350 eV.

The left of Figure 3 shows rippling in QCM mass-change during a measurement at fixed sputtering conditions. The vertical axis plots the mass accumulation, the slope of which gives the sputter yield. The short-term rippling was correlated with slight temperature variation in the QCM cooling loop. The effect of the rippling was to degrade our ability to determine the slope, thereby degrading measurement accuracy and sensitivity. To remedy this behavior we have upgraded our temperature controller to a unit from Polyscience that allows temperature control to better than 0.01 K. The right of Figure 3 shows a similar measurement with the new temperature controller and one can see that the rippling is significantly reduced. At typical conditions, the new temperature controller has improved sensitivity by a factor of approximately 3.

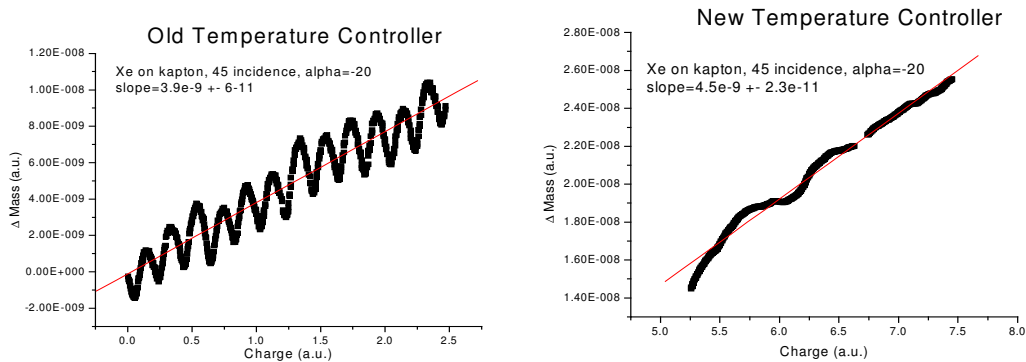


Figure 3 Left/Right: Mass change with old/new temperature controller. Xe ions on quartz at 350 eV.

In our recent measurements of insulators, e.g. boron nitride, we have observed effects of surface neutralization on the measured sputter yields. We have installed a Plasma Bridge Neutralizer (PBN) to remedy this problem. Below, we described a neutralization study and improvement associated with the PBN. Surface charging effects on BN sputtering have been previously observed by Zhang et al.²⁶. The left of Figure 4 shows the dependence of the HBC grade Boron Nitride sputter yield on the beam current at fixed beam voltage (prior to PBN installation). The reduction in sputter yield with increasing beam current was attributed to surface charging of the BN surface. At higher beam current more positive charge is accumulated on the sample surface and the charge repels beam ions thus reducing the measured sputter yield. These measurements were performed for 500 eV xenon ions at normal incidence with the QCM polar angle at 40 degrees from the surface normal. The right of Figure 4 shows measured sputter yield versus beam voltage (prior to PBN installation) at the same conditions. The arrow indicates the

sequence of the beam voltages, which was initially set to 500 V, then reduced to 350 V, 250 V, and 150 V, then increased back. Clearly hysteresis is observed since measured sputter yield values depend on the previous operating point. This phenomenon can be also explained by the surface charging. At higher beam voltage, the ion source generates higher beam current. Therefore, the amount of the electric charge accumulated on the sample surface depends on the previous operating condition; when the beam voltage and the beam current at the previous point are higher than at the present point, more charge is accumulated on the surface and the measured sputter yield is lower, and vice versa.

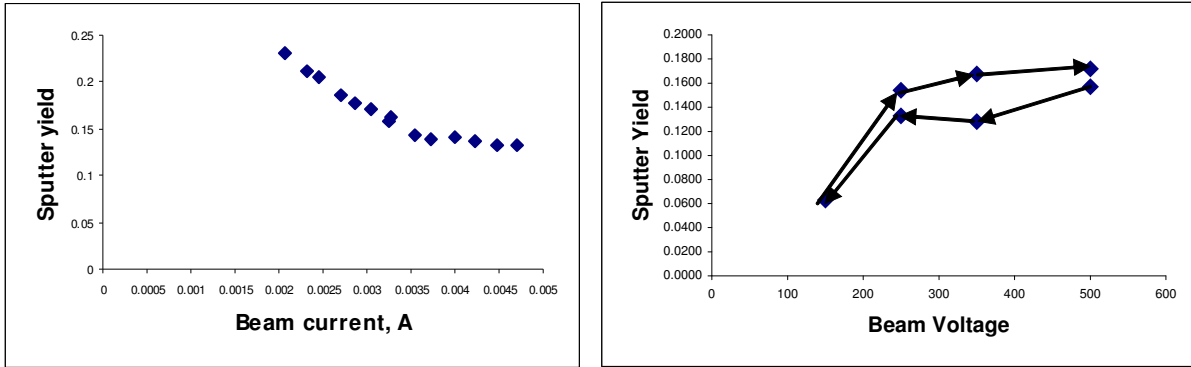


Figure 4 Left/Right: Sputter yield versus beam current (left) and voltage (right) before PBN installation.

In order to neutralize the surface charge, a plasma beam neutralizer (PBN) was placed in the chamber close to the sample being sputtered. The operating conditions of PBN are: emission current = 10-20 mA, Xe mass flow rate = 0.5 sccm. The PBN was biased negatively relative to ground potential and was set equal to the ion source neutralizer potential (typically -24 V). Measurements of the sputter yield with PBN operating shown in Figures 5 and 6 as function of current and beam voltage. As one can see in Figure 5 (in comparison to Figure 4), there is a significantly reduced dependence of the sputter yield on the beam current as well as substantial reduction in hysteresis. We also note that the measured sputter yields have increased compared to the previous results, which is in accordance with the proposed hypothesis of the surface charging.

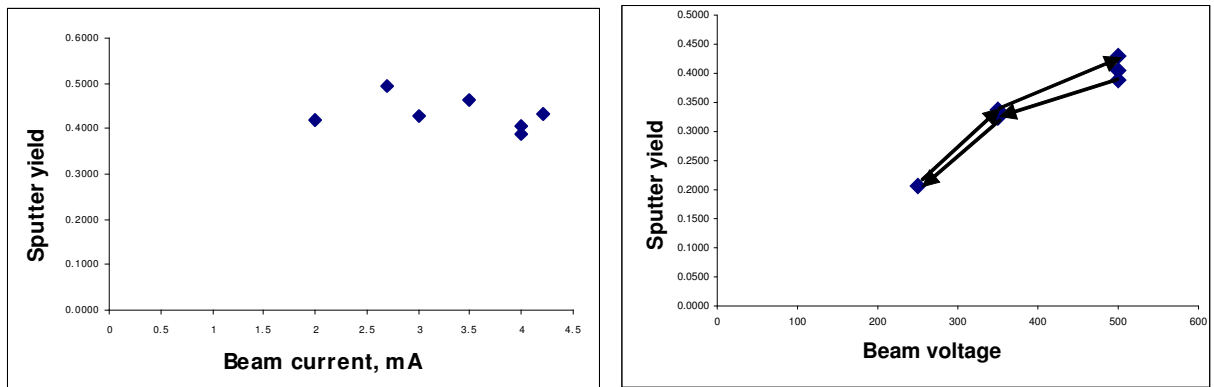


Figure 5 Left/Right: Sputter yield versus beam current (left) and voltage (right) after PBN installation.

C. Modified Zhang Expressions

For low ion energies and oblique incidence, sputtering profiles show azimuthal variation and are clearly not well described by azimuthally symmetric (diffuse) profiles of the form $y=Y\cos(\alpha)/\pi$ (or more generally $y\propto\cos(\alpha)^n$). While our measured profiles can be described with polynomials, it is preferable to use expressions that are based on theoretical considerations and contain fewer parameters. The availability of such expressions is limited; however Zhang et al. have published expressions for differential sputter yield profiles²⁵. Zhang's expressions are improvements of earlier expressions from Yamamura^{23,24}. As discussed in our past work^{6,7}, we have developed the use of Modified Zhang expressions which are essentially those of Zhang but where we adopt the use of two free fit

parameters. The first free parameter is the total sputter yield. We prefer to use as a free parameter, thereby decoupling the amplitude of the differential sputter yield profile from its shape. (Zhang’s expressions implicitly include the total yield, but it is calculated from material properties rather than appearing as an explicit parameter). Moreover, to obtain agreement between measurements and the Zhang expressions, we find that E_{th} (the threshold energy for sputtering) should be considered as a free fit parameter. We term this parameter as a “characteristic energy” E^* and our fits of experimental data show that it is not generally equal to the threshold energy. The resulting Modified Zhang (MZ) expression, y_{MZ} , is:

$$y_{MZ} = \frac{Y}{1 - \sqrt{\frac{E^*}{E}} \cos(\beta)} \cdot \frac{\cos(\alpha)}{\pi} \left[1 - \frac{1}{4} \sqrt{\frac{E^*}{E}} \left(\cos(\beta) \gamma(\alpha) + \frac{3}{2} \pi \sin(\beta) \sin(\alpha) \cos(\phi) \right) \right] \quad (2)$$

$$\gamma(\alpha) = \frac{3 \sin^2 \alpha - 1}{\sin^2 \alpha} + \frac{\cos^2 \alpha (3 \sin^2 \alpha + 1)}{2 \sin^3 \alpha} \ln \left(\frac{1 + \sin \alpha}{1 - \sin \alpha} \right)$$

where angles are as defined above and E is the ion energy. More recent work by Zhang et al. also discusses the use of a varying energy parameter, but in the context of expressions for energy distributions and total sputter yields²⁷. In general, rather than using the MZ expressions for *a priori* calculation, we treat Y and E^* as free fit-parameters which we determine from (least-squares fitting) experimental data. As shown below, the best-fit values of characteristic energy E^* vary with ion energy and incidence angle and generally do not equal E_{th} . Generally, we find that the MZ expressions used in this way provide a reasonable description of the shapes of the measured sputtered profiles (see Sections III-V and error calculations). We note that for high ion energy (limit $E \gg E^*$) the MZ expression reduces to the diffuse yield ($y = Y \cos(\alpha) / \pi$).

III. HBC Boron Nitride Sputter Yields

A. Total Sputter Yields of HBC BN

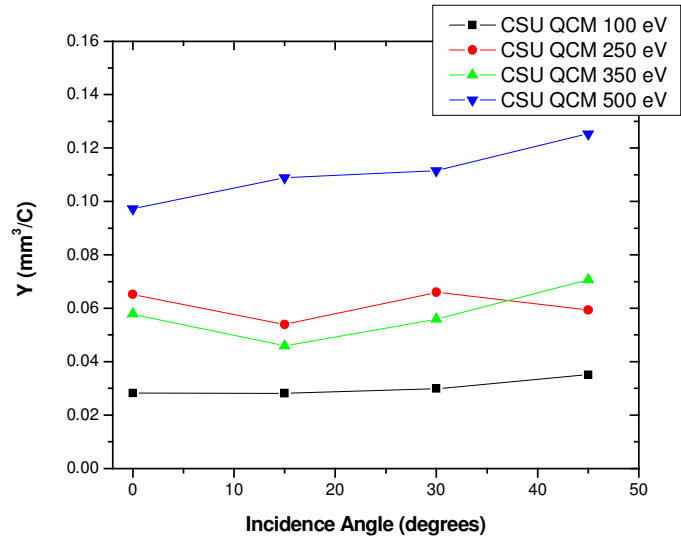
We have measured the sputtering of HBC grade boron nitride (BN) using the QCM system described above. The HBC BN is from GE’s Advanced Ceramics and corresponds to the graphite-like allotrope of BN. We have measured differential sputter yield profiles for HBC grade BN for incidence angles of 0, 15, 30 and 45 degrees and xenon ion energies of 100, 250, 350, and 500 eV. The measured profiles are least-squares fitted using the MZ expressions resulting in a total sputter yield (Y_{Cond}) and characteristic energy E^* . Values are given in Table 1. We provide the total sputter yields in units of mm^3/C , corresponding to the volume of sputtered material per coulomb of charge of bombarding ions. These units are preferable for multi-component materials since sputtered particles may have different identities (e.g. B, N, B_xN_y) and thus the units of “atoms/ion” are inappropriate.

Recall that the QCM measures only the components that **condense** and stick onto the QCM, which for BN corresponds to atomic boron, and B_xN_y clusters (including BN), but not nitrogen. Such a measurement accurately describes the sticking of sputtered particles to spacecraft surfaces (as would be of interest for deposition studies), especially if mass is considered by converting the volumetric yield to the directly measured mass yield (using the material density). **However, it may underestimate the sputtering from the target surface (as would be of interest in lifetime and erosion studies).** Owing to the likelihood of sputtering some atomic nitrogen during sputtering of BN, it is expected that the target-based yield is higher than the QCM yield. Accordingly, we label the experimentally measured yield as Y_{Cond} , the value of which describes condensable components (assumed to be BN) and provides a lower bound of the sputter yield from the target surface. Additionally, we compute an upper bound of the target-based yield, Y_{Target_Max} , by assuming that all sputtering is as atomic boron and nitrogen, and that for each boron atom condensed on the QCM there is a sputtered nitrogen atom that did not condense. ($Y_{Target_Max} = 2.30 \times Y_{Cond} = ((M_B + M_N) / M_B) \times Y_{Cond}$, where M_B and M_N are atomic masses of B and N respectively). Note that for the case of a mixture of atom and cluster sputtering the true target yield would lie between the condensable yield (Y_{Cond}) and the maximum yield (Y_{Target_Max}). Mass spectrometry results [1] and multi-component sputtering theory suggest sputtering predominantly as atoms, and therefore Y_{Target_Max} **is expected to be the more accurate value** for target-based yields.

Table 1 Total Sputter Yields (Y) and Characteristic Energies (E^*) of HBC BN

Ion Energy (eV)	Incidence Angle (Deg)	Y_{Cond} (mm ³ /C)	Y_{Target_Max} (mm ³ /C)	E^* (eV)	Error (Avg, Normalized)
100	0	0.0123	0.0283	19.0	0.22
100	15	0.0122	0.0283	18.1	0.10
100	30	0.0130	0.0299	17.7	0.10
100	45	0.0153	0.0351	14.3	0.14
250	0	0.0283	0.0651	104	0.27
250	15	0.0234	0.0539	65.2	0.13
250	30	0.0287	0.0660	96.1	0.12
250	45	0.0258	0.0594	86.4	0.12
350	0	0.0251	0.0578	88.1	0.11
350	15	0.0200	0.0459	97.0	0.15
350	30	0.0243	0.0559	148	0.12
350	45	0.0308	0.0707	163	0.12
500	0	0.0423	0.0973	123	0.10
500	15	0.0473	0.109	150	0.13
500	30	0.0485	0.112	207	0.11
500	45	0.0545	0.125	231	0.10

Figure 6 plots the total sputter yields of Table 1. The plotted yields are the values of Y_{Target_Max} . For fixed energy we find that the yield generally increases with incidence angle as is typical in this angular range. (Generally sputtering increases with incidence angle until a maximum at approximately 40-60 degrees of incidence.) We note that the dependence on angle is weaker than what is typically observed in metals, though we have observed similar behavior in kapton. An apparent anomaly in the data is the higher sputter yields at 250 eV as compared to 350 eV. This behavior is repeatable and we believe it to be physically real. The mechanisms for this have not been determined, but it is possibly due to changes in composition of the sputtered particles at the different energies; for example, more sputtering of B and N at 350 eV as compared to more sputtering of BN at 250 eV.

**Figure 6. Total sputter yields for HBC BN due to Xenon ions.**

Where possible, we compare the measured yields (Y_{Target_Max}) with those from the limited published measurements. The left of Figure 7 shows our 350 eV measurements along with weight loss measurements by a French research group²⁸ and a profilometry measurement by NASA GRC²⁹ at similar energy. Neither group specifies the grade of BN used. We view the agreement with other data as reasonable especially given possible material variation, surface effects etc. The right of Figure 7 shows comparison with measurements by the French group at 500 eV and also shows reasonable agreement. (The nearly monotonic increase of sputter yield with incidence angle for angles as high as 80 degrees in the French data is atypical.) The fact that our values tend to be higher than the published values may be due to the presence of clusters in the sputtering (in which case the true value of the target yield is less than Y_{Target_Max} as discussed above Table 1), however the difference may also be due to experimental errors, target conditions etc. Note that the lowest sputtering energies reported in these comparison

studies were 300 eV by GRC and 350 eV by the French group, and apart from our own work we are not aware of other measurements below 300 eV.

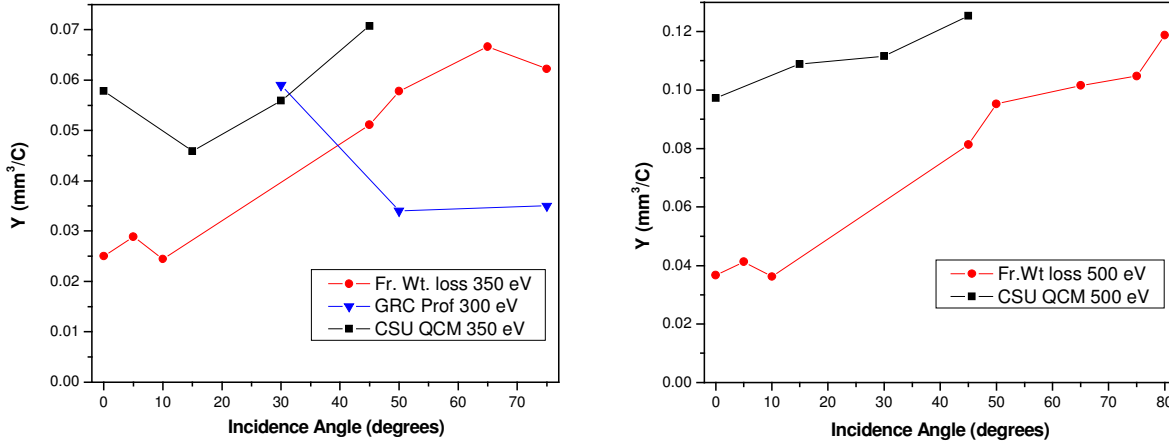


Figure 7. Left: Total sputter yields for HBC BN as compared with published values. See text.

We can also compare the total sputter yields of HBC BN measured by our QCM apparatus with past CSU weight loss measurements. We find that the past weight loss measurements are lower, by a factor of approximately 2 to 3, than the condensable component of the present QCM measurements. The reasons for this are under investigation, and we hypothesize that surface charge neutralization may have been insufficient in our past weight loss measurements. Comparison of QCM yields with accurate weight loss measurements would be informative to better understand the condensable fraction of sputter products that are condensable. The comparison with published values as well as our positive agreement between the QCM and weight-loss measurements for other materials gives us confidence in the QCM measurements presented here.

B. Differential Sputter Yield Measurements of HBC BN

Using our QCM system we have measured differential sputter yields for HBC grade BN for incidence angles of 0, 15, 30 and 45 degrees and xenon ion energies of 100, 250, 350, and 500 eV. We provide the results in the context of the fitted MZ expressions. Rigorously speaking, the QCM measurements must be interpreted as giving the angular sputtering profiles of only condensable products, though to first approximation it is reasonable to assume that they provide a description of all sputter products. Included in Table 1 are values for the characteristic energy E^* , which governs the profile shape via equation (2) as discussed above. To characterize the agreement between the fitted MZ profiles and the measured data, we also provide an error column, which we compute as the average (absolute) difference between the measured points and corresponding fitted points, normalized by the maximum measured yield.

Examples of comparison between measured (raw) QCM data and fitted MZ profiles are given in Figure 8 (in arbitrary units, but the same scale for both plots). Both plots are for xenon ion energies of 350 eV, with the left plot being at normal incidence and the right plot being at 30 degrees incidence. The plots include: QCM measured points, best-fit MZ profiles, and (for comparison) diffuse profiles with the same total yield. One can see relatively good agreement between the measured profiles and MZ profiles (see also numerical error values in Table 2). The normally incident profile is azimuthally symmetric. The profile for 30 degrees incidence is measured in the forward/backward plane ($\phi=0,180$ degrees) and shows a forward sputter lobe (negative alpha) and reduced sputtering in the backward direction (positive alpha). As we have found for other materials, the MZ expressions provide a reasonable description of the measured profiles, but tend to predict a slightly broader and lower amplitude forward-sputter lobe^{6,7}.

In Figure 9 we plot (using colored hemispheres) the best-fit Zhang differential sputter yields for each of the measured cases. Colors (indicated in legend) correspond to the yield in the given direction. Here we focus on the shape (not magnitude) of the profiles; therefore, we normalize the differential sputter yields by the total sputter yields (or equivalently assume total sputter yields of unity).

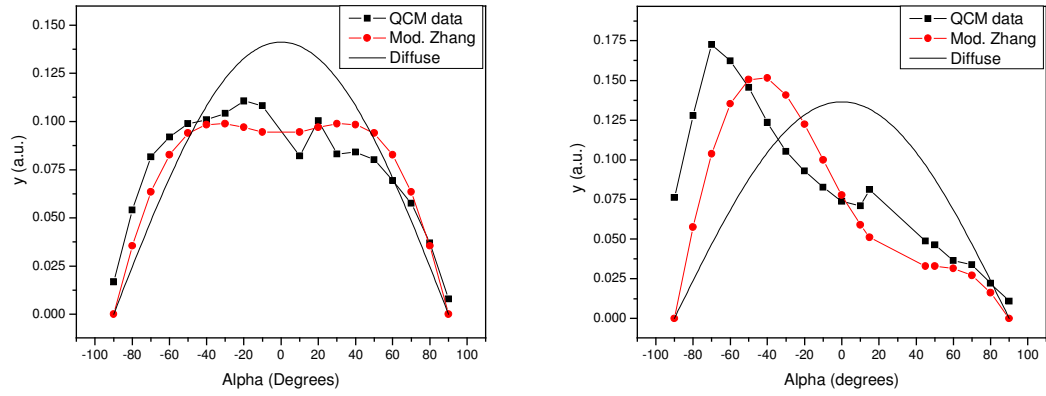


**Figure 8. Comparison of QCM data with MZ profiles for 350 eV ions.
Left: Normal incidence. Right: 30 degrees incidence.**

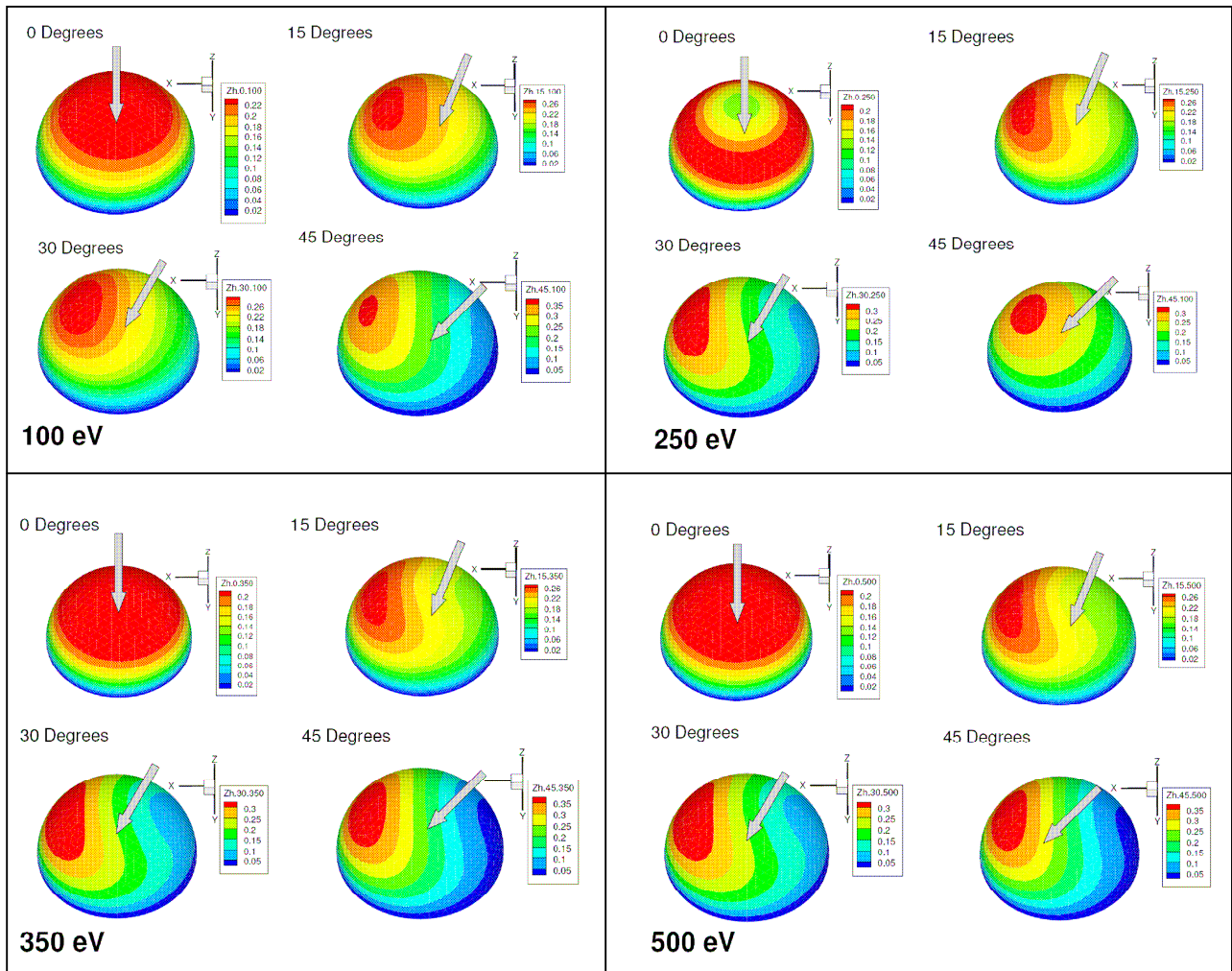


Figure 9. Normalized differential sputter yield profiles for xenon ions on HBC BN.

IV. Total and Differential Sputter Yield Measurements of Quartz

A. Total Sputter Yields of Quartz

This section reports sputtering measurements of quartz and follows a similar structure to that used for BN in Section III. The quartz (CVI) was in the form of 2"x2" substrates. Using our QCM system we have measured sputter yields for incidence angles of 0, 15, 30 and 45 degrees and xenon ion energies of 100, 250, 350, and 500 eV. Table 2 provides the total sputter yields in units of mm^3/C found from eqn. (1). Again, we use both Y_{Cond} and $Y_{\text{Target_Max}}$. Here we consider SiO_2 as the condensable from SiO_2 and assume atom sputtering (with detection of Si but not O) for the maximum yield case, i.e. $Y_{\text{Target_Max}} = 2.14 \times Y_{\text{Cond}} = (M_{\text{Si}} + 2M_{\text{O}}) / M_{\text{Si}} \times Y_{\text{Cond}}$. $Y_{\text{Target_Max}}$ is expected to be the more accurate value for target-based yields (see also discussion of Figure 10).

Table 2 Total Sputter Yields (Y) and Characteristic Energies (E^*) of Quartz

Ion Energy (eV)	Incidence Angle (Deg)	Y_{Cond} (mm^3/C)	$Y_{\text{Target_Max}}$ (mm^3/C)	E^* (eV)	Error (Avg, Normalized)
100	0	0.0098	0.0209	10.0 ¹	0.24
100	15	0.0061	0.0130	20.2	0.17
100	30	0.0126	0.0269	34.7	0.22
100	45	0.0154	0.0329	42.7	0.15
250	0	0.0367	0.0786	68.1	0.23
250	15	0.0333	0.0713	83.8	0.10
250	30	0.0547	0.117	111	0.12
250	45	0.0875	0.187	137	0.14
350	0	0.0398	0.0850	140.9	0.09
350	15	0.0461	0.0985	70.5	0.16
350	30	0.0869	0.186	146	0.09
350	45	0.131	0.280	178	0.12
500	0	0.0706	0.151	147	0.10
500	15	0.0628	0.134	83.9	0.23
500	30	0.116	0.250	206	0.08
500	45	0.151	0.322	245	0.12

¹- Note that for 100 eV at 0 incidence, the data is best fit in the limit of E^* goes to zero (i.e. $E^*/E \ll 1$ as is the case for diffuse yields), but we report $E^*=10$ eV since it gives essentially the same profile and avoids singularities.

Figure 10 plots the total sputter yields ($Y_{\text{Target_Max}}$) of Table 2. For fixed energy we find that the yield generally increases with incidence angle as is typical in this angular range. We also compare the total sputter yields of silicon measured by our QCM apparatus with past CSU weight loss measurements. Figure 10 shows also the weight loss data and indicates reasonable agreement between the two methods. (Matching colors are used to aid the reader: 250 eV data is in red, 350 eV data is in green.) The fact that the QCM values of $Y_{\text{Target_Max}}$ tend to be higher than the weight-loss values may be due to the presence of clusters in the sputtering, a hypothesis which is consistent with the fact that all weight loss measurements are between the corresponding values of $Y_{\text{Target_Max}}$ and Y_{Cond} .

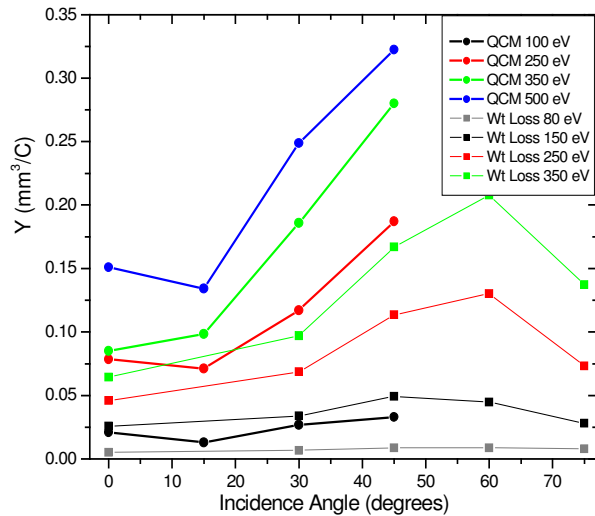


Figure 10. Total sputter yields of quartz. See text.

B. Differential Sputter Yield Measurements of Quartz

We have measured differential sputter yields for quartz for incidence angles of 0, 15, 30 and 45 degrees and xenon ion energies of 100, 250, 350, and 500 eV. Differential sputter yield measurements for silicon are performed and analyzed in the analogous manner to those for HBC BN. Table 2 includes the corresponding values of characteristic energy E^* and error (computed as for Table 1). Examples of comparison between measured (raw) QCM data and fitted MZ profiles are given in Figure 11 (incidence of 0° and 30°). Figure 12 shows (using colored hemispheres) the differential sputter yields for each of the measured cases (with total yields normalized to unity).

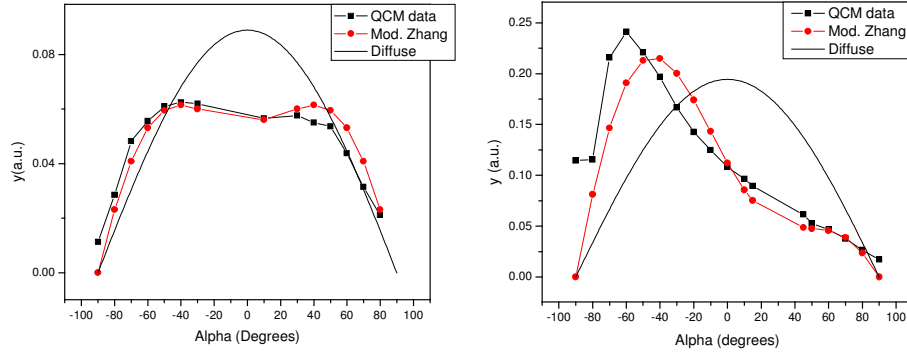


Figure 11. Comparison of QCM data with best-fit MZ profiles for 350 eV ions. Left: $\beta=0^\circ$, right $\beta=30^\circ$.

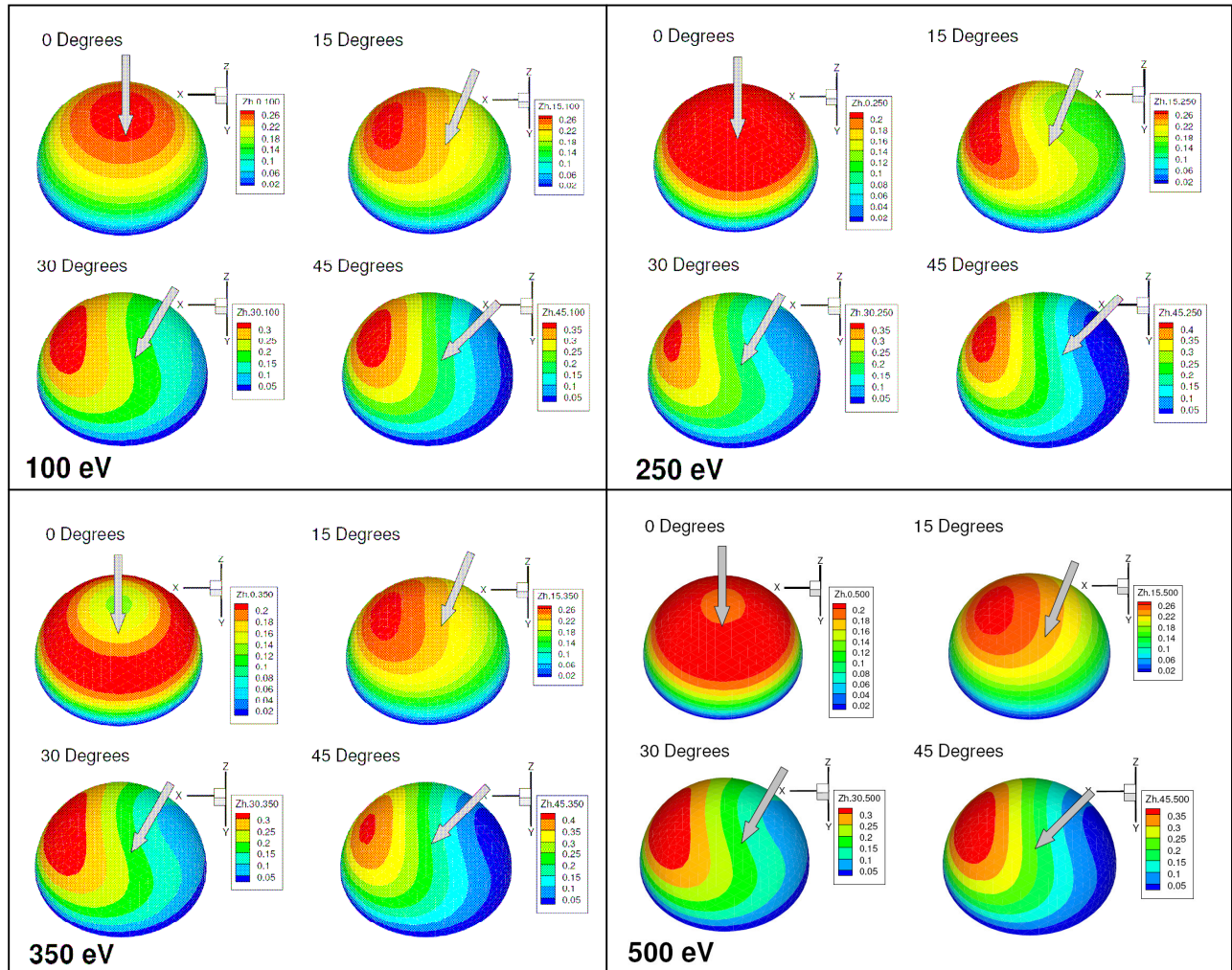


Figure 12. Normalized differential sputter yield profiles for xenon ions on quartz.

V. Total and Differential Sputter Yield Measurements of Kapton

A. Total Sputter Yields of Kapton

This section reports sputtering measurements of kapton and follows a similar structure to those used for BN and quartz. We have tested a polyamide film with trade name Kapton HN (Dupont). Using our QCM system we have measured sputter yields for incidence angles of 0, 15, 30 and 45 degrees and xenon ion energies of 250, 350, and 500 eV. Measurements for 100 eV ions had poor signal-to-noise owing to the low density and sputtering of kapton, and are not reported. Table 3 provides the total sputter yields in units of mm^3/C found from eqn. (1). Again, we use both Y_{Cond} and $Y_{\text{Target_Max}}$. The chemical formula for kapton (polyamide) is $(\text{C}_{22}\text{H}_{10}\text{N}_2\text{O}_5)_n$ so that in the absence of other information we consider $\text{C}_{22}\text{H}_{10}\text{N}_2\text{O}_5$ as the condensable from kapton and assume atom sputtering (with detection of only C) for the maximum yield case, i.e. $Y_{\text{Target_Max}} = 1.45 \times Y_{\text{Cond}} = (22M_C + 10M_H + 2M_N + 5M_O) / 22M_C \times Y_{\text{Cond}}$. $Y_{\text{Target_Max}}$ is expected to be the more accurate value for target-based yields (see also discussion of Figure 13).

Table 3 Total Sputter Yields (Y) and Characteristic Energies (E*) of Kapton

Ion Energy (eV)	Incidence Angle (Deg)	Y_{Cond} (mm^3/C)	$Y_{\text{Target_Max}}$ (mm^3/C)	E^* (eV)	Error (Avg, Normalized)
250	0	0.0084	0.0122	121.9	0.21
250	15	0.0094	0.0138	83.9	0.17
250	30	0.0112	0.0164	83.6	0.17
250	45	0.0136	0.0197	90.3	0.15
350	0	0.0143	0.0208	93.2	0.2
350	15	0.0295	0.0428	174	0.48
350	30	0.0201	0.0293	176.9	0.17
350	45	0.0278	0.0405	198.3	0.13
500	0	0.0297	0.0433	258.2	0.23
500	15	0.0372	0.0541	288	0.19
500	30	0.0454	0.0658	282.1	0.14
500	45	0.0445	0.0644	283	0.11

Figure 13 plots the total sputter yields ($Y_{\text{Target_Max}}$) of Table 2. We find that the dependence on incidence angle is weaker for kapton that is typical for other materials. We compare the total sputter yields of kapton measured by our QCM apparatus with past CSU weight loss measurements. Figure 13 shows also the weight loss data and indicates reasonable agreement between the two methods. (Matching colors are used to aid the reader: 250 eV data is in red, 350 eV data is in green.) As with quartz, we find that the QCM values of $Y_{\text{Target_Max}}$ tend to be higher than those from weight-loss but that the weight loss is (approximately) between the QCM lower and upper bounds of Y_{Cond} and $Y_{\text{Target_Max}}$. This result provides validation of the QCM measurement and suggests that the kapton sputtering contains some non-condensable fraction.

B. Differential Sputter Yield Measurements of Kapton

We have measured differential sputter yields for quartz for incidence angles of 0, 15, 30 and 45 degrees and xenon ion energies of 250, 350, and 500 eV. Differential sputter yield

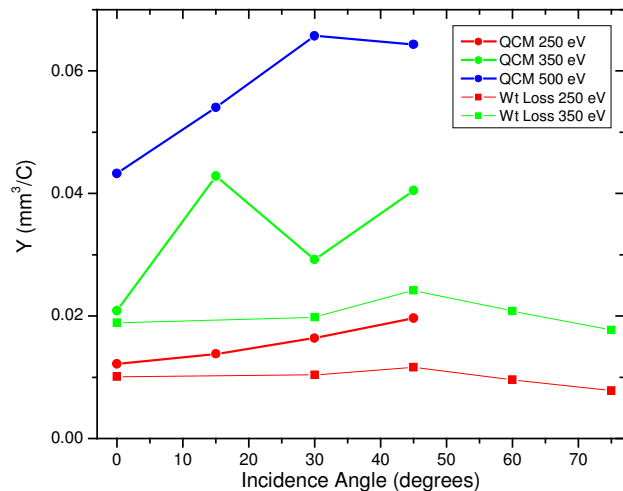


Figure 13. Total sputter yields of kapton. See text.

measurements for silicon are performed and analyzed in the analogous manner to those for HBC BN. Table 3 includes the corresponding values of characteristic energy E^* and error (computed as for Table 1). Examples of comparison between measured (raw) QCM data and fitted MZ profiles are given in Figure 14 (incidence of 0° and 30°). The larger noise (as compared to BN and quartz) is due to the lower sputter yields and density of kapton. Figure 15 shows (using colored hemispheres) the differential sputter yields for each of the measured cases (with total yields normalized to unity).

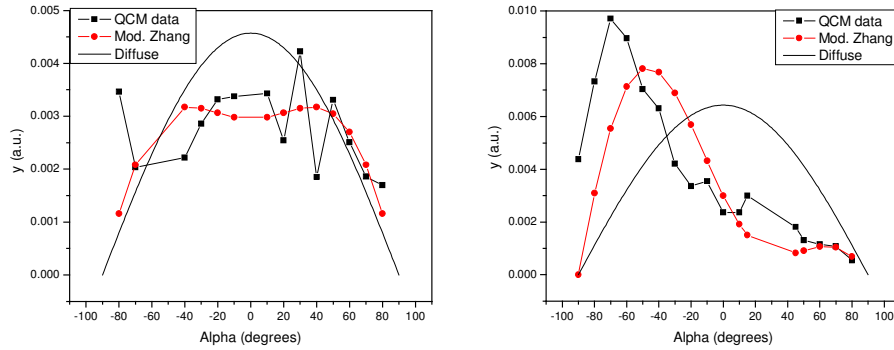


Figure 14. Comparison of QCM data with best-fit MZ profiles for 350 eV ions. Left: $\beta=0^\circ$, right $\beta=30^\circ$.

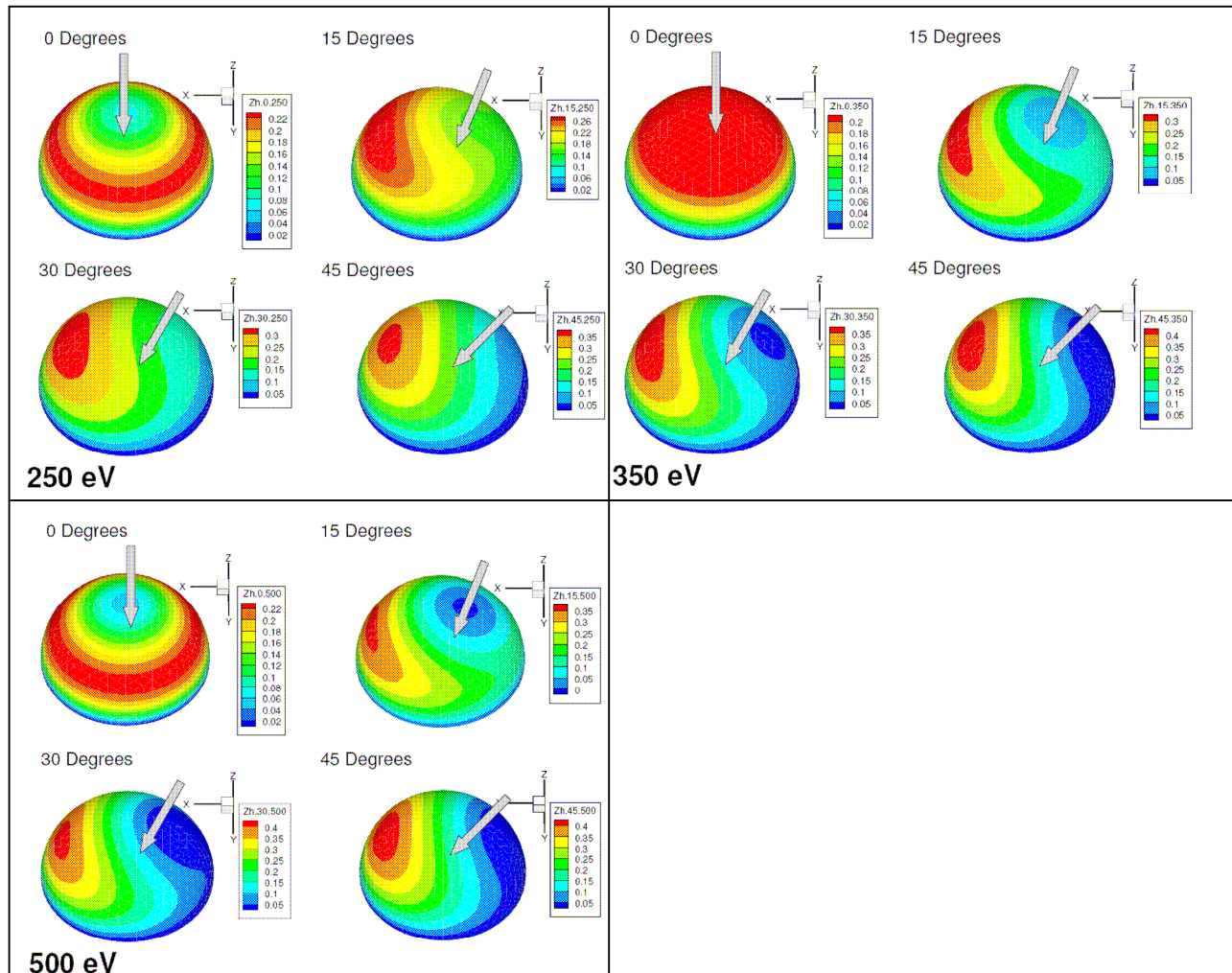


Figure 15. Normalized differential sputter yield profiles for xenon ions on Kapton.

VI. Conclusions

We have reported total and differential sputter yield measurements for HBC grade boron nitride (BN), quartz, and kapton using a QCM measurement system. We provide measurements of sputter yield profiles for xenon ions incident on pre-sputtered targets at a range of incidence angles and ion energies. Because the QCM measures only condensable components, the directly measured yields provide a lower bound on the target sputter yield. Accordingly, we also compute an upper bound under the assumption that all sputtering is as atoms and that we measure only the condensable atoms (e.g. assuming that BN sputters as atomic B and N, yet we only measure B). In this way we obtain a range of yield values at each condition, though we anticipate that the true target based value is closer to the upper bound. In terms of deposition (contamination) of sputter products onto spacecraft surfaces, the QCM measurement provides a true measurement, especially if one uses the material density to convert the volumetric yield to a mass yield (which is the quantity directly measured by the QCM).

We observe that sputtering of boron nitride is particularly sensitive to surface charging effects that can significantly change the measured yields (owing to repulsion of the ion beam). These effects are mitigated through appropriate neutralization. The measured total sputter yields for HBC BN are found to be in rough agreement with the limited values available from the literature. For measurement of quartz and kapton we compare the total sputter yields with weight loss measurements (from past work in our laboratory) and find reasonable agreement. The differential sputter yields (angular profiles) for all materials are markedly anisotropic for the ion energies studied and are reasonably described with Modified Zhang (MZ) expressions. Clearly any modeling of the trajectories of sputtered particles for these species at these conditions should not assume a simple diffuse form of the differential sputter yield. Using the parameters for total yield and characteristic energy given in the tables, the MZ expressions can easily be used to compute the differential sputter yields.

With the improvements to the measurement system presented in this work, the QCM provides a useful tool for measurement of differential sputter yields for materials of interest to EP. In contrast to techniques such as cavity ring-down spectroscopy, the QCM approach is not amenable to real-time *in situ* measurements, on the other hand the system allows detailed angular measurements from which differential and total sputter yields can be readily inferred. Currently, the detection limit of the system allows measurement of yields for ion energies as low as ~100 eV, a level difficult to attain with other measurement techniques and systems. For example, to our knowledge sputtering of BN has not previously been measured in this energy range with past measurements limited to minimum ion energy of 300 eV. With further improvements in sensitivity (and to the ion beams) we aim to measure sputter yields for lower energies closer to the sputtering threshold, i.e. in the energy range of 50-100 eV. Also interesting would be to study the variation in sputter yields as a function of target temperature, and to make further comparisons between QCM measurements and weight loss measurements to examine the condensable fraction and better understand the identities of the sputtered particles (atoms, clusters).

Acknowledgments

The authors would like to thank Air Force Research Labs (Edwards Air Force Base, CA) for funding support. The authors also thank Paul Wilbur (Colorado State University) for initial development of the QCM apparatus, Lubos Brieda (Air Force Research Labs) for providing the meshing used to prepare the hemispherical plots, and Steen Vecci (Colorado State University) for assistance maintaining the QCM apparatus.

References

- ¹Betz G and Wien K 1994 Energy and angular distributions of sputtered particles International *J.Mass Spectrometry and Ion Processes* 140 1-110
- ²Tartz M, Neumann H, Fritsche B, Leiter H, and Esch J 2004 Investigation of sputter behaviour of ion thruster grid materials 40th Joint Propulsion Conference AIAA Paper 2004-4114
- ³Kolasinski R D 2005 Oblique angle sputtering yield measurements for ion thruster grid materials 41st Joint Propulsion Conference AIAA paper 2005-3526
- ⁴Kolasinski R D, Polk J E, Goebel D and Johnson L J 2006 Carbon sputtering yield measurements at grazing incidence 42nd AIAA/ASME/SAE/ASEE Joint Propulsion Conference (Sacramento, CA) AIAA 2006-4337

- ⁵Zoerb K A, Williams J D, Williams D D and Yalin A P 2005 Differential sputtering yields of refractory metals by xenon, krypton, and argon ion bombardment at normal and oblique incidences 29th International Electric Propulsion Conference (Princeton, NJ) IEPC-2005-293
- ⁶Yalin A P, Williams J D, Surla V, Wolf J and Zoerb K A 2006 Azimuthal differential sputter yields of molybdenum by low energy ion bombardment *42nd AIAA/ASME/SAE/ASEE Joint Propulsion Conference* (Sacramento, CA)
- ⁷Yalin A P, Williams J D, Surla V, and Zoerb K A 2007 Differential Sputter Yield Profiles of Molybdenum due to Bombardment by Low Energy Xenon Ions at Normal and Oblique Incidence” *Journal of Physics D – Applied Physics* 40 3194-3202
- ⁸Polk J E 1999 An overview of the results from an 8200 hour wear test of the NSTAR ion thruster paper 35th Joint Propulsion Conference AIAA Paper 99-2446
- ⁹Yalin A P, Surla V, Farnell C, Butweiller M, and Williams J D 2006 Sputtering Studies of Multi-Component Materials by Weight Loss and Cavity Ring-Down Spectroscopy, *42nd AIAA Joint Propulsion Conference* (Sacramento, CA)
- ¹⁰Chiplonkar V T and Rane S R 1965 Dependence of angular distribution of sputtering by positive ions from metal targets on the impact angle *Indian J. Pure Appl Phys* 3 161
- ¹¹Tsuge H and Esho S 1981 Angular distribution of sputtered atoms from polycrystalline metal targets *J. Appl. Phys.* 52 4391-95
- ¹²Wucher A and Reuter W 1988 Angular distribution of sputtered particles from metals and alloys *J. Vac. Sci. Tech. A* 6 (4) 2316-18
- ¹³Mannami M, Kimura K and Kyoshima A 1981 Angular distribution measurements of sputtered Au atoms with quartz oscillator microbalances *Nuclear Instruments and Methods* 185 533-37
- ¹⁴Wickersham C E and Zhang Z 2005 Measurement of angular emission trajectories for magnetron-sputtered tantalum *Jnl. Electronic Materials* 34
- ¹⁵Shutthanandan V, Ray P, Shivaparan N, Smith R, Thevuthasan T and Mantenicks M 1997 On the measurement of low-energy sputtering yield using rutherford backscattering spectrometry *25th International Electric Propulsion Conference* (Cleveland, OH) IEPC-97-069
- ¹⁶Mantenicks M, Foster J, Ray P, Shutthanandan S, and Thevuthasan T 2001 Low energy xenon ion sputtering yield measurements *27th International Electric Propulsion Conference* (Pasadena, CA) IEPC-01-309
- ¹⁷Kundu S, Ghose D, Basu D, Karmohapatro S B 1985 The angular distribution of sputtered silver atoms *Nuclear Instruments and Methods in Physics Research B* 12 352-57
- ¹⁸Surla V and Yalin A P 2007 Differential sputter yield measurements using cavity ring-down *Applied Optics*, 44, 30, pp. 6496-6505
- ¹⁹Sigmund P 1969 Theory of sputtering I: sputtering yield of amorphous and polycrystalline targets *Phys. Rev.* 184 383-416
- ²⁰Wehner G K and Rosenberg D 1960 Angular distribution of sputtered material *J. App. Phys.* 31 177-9
- ²¹Chini T K Tanemura M and Okuyama F 1996 Angular distribution of sputtered Ge atoms by low keV Ar+ and Ne+ ion bombardment *Nucl. Instr. and Methods in Physics Research B* 119 387-91
- ²²Yamamura Y and Muraoka K 1989 Over-cosine angular distributions of sputtered atoms at normal incidence *Nucl. Instr. and Methods in Physics Research B* 42 175-81
- ²³Yamamura Y 1981 Contribution of anisotropic velocity distribution of recoil atoms to sputtering yields and angular distributions of sputtered atoms *Rad. Eff.* 55 49–55
- ²⁴Yamamura Y 1982 Theory of sputtering and comparison to experimental data *Nucl. Instr. and Meth.* 194 515–22
- ²⁵Zhang Z L and Zhang L 2004 Anisotropic angular distributions of sputtered atoms *Radiation Effects and Defects in Solids* 159 301-07
- ²⁶Zhang J. et al. 1997 Sputtering investigation of boron nitride with secondary ion and secondary neutral mass spectrometry *J. Vac. Sci. Tech. A* 15 (2) 243-247
- ²⁷Zhang L and Zhang L Z 2005 Anisotropic energy distribution of sputtered atoms induced by low energy heavy ion distribution *Rad. Effects & Defects in Solids* 160 337-47
- ²⁸Garnier Y et al. 1999 Low-energy xenon ion sputtering of ceramics investigated for stationary plasma thrusters *J. Vac. Sci. Tech. A* 17 (6) pp. 3246-3254
- ²⁹Britton M. et al 2002 Sputtering erosion measurements on boron nitride as a Hall thruster material *NASA/TM* 2002-211837